Short-pulse high-intensity laser-generated fast electron transport into thick solid targets

J. R. Davies, A. R. Bell, and M. G. Haines
Blackett Laboratory, Imperial College, London SW7 2BZ, United Kingdom

S. M. Guérin
Centre de Physique Théorique, CNRS, Ecole Polytechnique, 91128 Palaiseau Cedex, France
(Received 9 July 1997)

The transport of fast electrons generated by 1 ps, 1 μm wavelength laser pulses focused to spot diameters of 20 μm and peak intensities of up to 2×10^{18} W cm^{-2} on to solid aluminum targets is considered using a relativistic Fokker-Planck equation, which is solved by reducing it to an equivalent system of stochastic differential equations. The background is represented by $\mathbf{E}=\eta\mathbf{j}_b$, where η is the resistivity and $\mathbf{j}_b$ is the background current density. Collisions, electric and magnetic fields, and changes in resistivity due to heating of the background are included. Rotational symmetry is assumed. The treatment is valid for fast electron number densities much less than that of the background, fast electron energies much greater than the background temperature, and time scales short enough that magnetic diffusion and thermal conduction are negligible. The neglect of ionization also limits the validity of the model. The intensities at which electric and magnetic fields become important are evaluated. The electric field lowers the energy of fast electrons penetrating the target. The magnetic field reduces the radial spread, increases the penetration of intermediate energy fast electrons, and reflects lower energy fast electrons. Changes in resistivity significantly affect the field generation. The implications for $K\alpha$ emission diagnostics are discussed. [S1063-651X(97)10412-3]

PACS number(s): 52.40.Nk, 52.50.Jm, 52.70.La

I. INTRODUCTION

This paper considers the transport of fast electrons (kinetic energies $K>10$ keV) into thick, solid targets in picosecond laser solid interactions. Numerous experimental and theoretical works have been published on the generation and transport of such fast electrons over the past 20 years. An extensive summary of fast electron temperatures, determined from x-ray emission measurements from laser solid experiments prior to 1986, is given by Gitomer *et al.* [1]. Summaries including more recent experimental and theoretical determinations of fast electron temperatures are given by Gibbon and Förster [2] and Lee [3]. These show a general trend in fast electron temperatures given by $(I\lambda^2)^{\alpha}$, with $\alpha=0.3$–0.5 and temperatures of order 100 keV at $I\lambda^2\sim10^{17}$ W cm$^{-2}\mu$m^2. No clear trend is apparent in the fraction of absorbed energy found to be in the fast electrons, values in the range 1–100 % being suggested [1,3–14]. However most fall in the range 10–50 %.

The results that are of interest here are measurements of $K\alpha$ emission from layered targets, e.g., [3–10]. These show that electrons with energies $>$keV are present at depths of many micrometers in solid targets. The interpretation of these experiments requires a model for the electron transport into the target. Most of these experiments have been interpreted using models including only collisional effects. Spencer's results [15] for electron transport are commonly used. These results are for an electron source in an infinite, uniform medium, whereas in laser solid experiments there is always at least one boundary, from which the electrons enter. Luther-Davies *et al.* [5] showed that the inclusion of reflective boundaries in their Monte Carlo transport code, which were consistent with their experimental results, produced results quite different from Spencer's model. Other experiments have also been interpreted using Monte Carlo codes, e.g., [6,7]. These models ignore the effect of electric and magnetic fields generated in the target. In effect they assume that the target has zero resistivity and infinite electron density, so that the fast electron current remains exactly balanced by a cold electron return current which has no energy and generates no field. These will be reasonable approximations as long as the flux of fast electrons is small, which will be true at low intensities, and the target resistivity is low. These approximations need careful evaluation in light of more detailed models. Here we will try to address the effect of finite resistivity.

Luther-Davies *et al.* [5] mention that a magnetic field might be present in the target. They state that including a fixed magnetic field in their Monte Carlo code increased the penetration depth of low energy electrons, but they give no other details.

PIC and Vlasov codes can model fast electron transport including electric and magnetic field generation, and some PIC codes include collisions, e.g., [16,17]. However, these codes have difficulty with large scales, low temperatures, and high densities. Consequently their use has largely been limited to modelling the fast electron generation, e.g., see [2], coronal transport, e.g., [18], and very thin targets, e.g., [17].

Tabak *et al.* [19] have considered the transport of fast electrons including electric and magnetic fields, using the code ANTHEM [20] and a simple one-dimensional model, but for a very different situation form the ones considered here.

The effect of electric fields has been considered in one-dimensional models. Glinsky [21] gives a one-dimensional, two-fluid model for fast electron transport through a cold electron background, which he compares with LASNEX [22] simulations. He finds that the electric field dominates the

transport at early times. He uses the Spitzer resistivity, which is of limited validity at the high densities and low temperatures in which we are interested. Bell *et al.* [23] give an analytic solution to a similar one-dimensional model of electron transport, including only the electric field. They assume that the resistivity is uniform and constant. For parameters typical of solid density aluminum the mean penetration depth they obtain is less than that from a purely collisional model for absorbed intensities $>10^{17}$ W cm^{-2}.

Glinsky [21] estimates the magnetic field generated by a cylinder of fast electrons entering a target. The radial variation in the axial electric field leads to a rapidly growing, azimuthal magnetic field. The force exerted by the magnetic field on the fast electrons can rapidly exceed that of the electric field. A consistent calculation of the magnetic field requires a two-dimensional treatment.

The propagation of electron beams in plasmas, including only the electric and magnetic fields, has been the subject of much study. These treatments were concerned with the firing of charged particle beams through preformed plasmas and they differ from our situation in which the electrons are generated from the plasma. Miller's book [24] reviews such treatments. Magnetic fields have a major effect on the dynamics of such beams, causing pinching of the beam, filamentation, kink (or hosing), and sausage (or bunching) instabilities.

To model the effects of fields and collisions we treat the fast electrons relativistically, using a Fokker-Planck equation expressed by a formally equivalent system of stochastic differential equations (SDEs), which we solve using the standard Monte Carlo–type method. The background electrons are represented by $\mathbf{E}=\eta\,\mathbf{j}_b$, as in the treatments of field generation mentioned above [21,23,24]. In effect, the fast electrons are treated as particles and the background electrons as a cold, stationary fluid. Changes in resistivity due to Ohmic and collisional heating of the background are included. We assume rotational symmetry, as appropriate to the case of a circular laser spot. The laser interaction is not dealt with, a specified distribution of fast electrons being generated. As this distribution is not well known, we cannot make detailed predictions and instead try to establish what sort of effects could be expected and when they would be important.

The equations used are discussed in the next section and the computational approach is outlined in Sec. III. The transport of fast electrons generated by a picosecond, 20 μm diameter laser spot, at a range of intensities, incident on a solid aluminum target is discussed in Sec. IV. Section V summarizes the main points.

II. THE MODEL

Neglecting the motion of the background particles, collisions between fast electrons and large angle scattering gives a Fokker-Planck equation,

$$\frac{\partial f}{\partial t}=-\frac{\partial}{\partial \mathbf{r}}\cdot(\mathbf{v}f)-\frac{\partial}{\partial \mathbf{p}}\cdot[(\mathbf{F}+\langle\Delta\mathbf{p}\rangle)f]+\frac{1}{2}\frac{\partial}{\partial \mathbf{p}}\frac{\partial}{\partial \mathbf{p}}:(\langle\Delta\mathbf{p}\Delta\mathbf{p}\rangle f), \tag{1}$$

$$\mathbf{F}=-e(\mathbf{E}+\mathbf{v}\times\mathbf{B}),$$

$$\langle\Delta\mathbf{p}\rangle=\left(\langle\Delta p\rangle-\frac{p}{2}\langle\Delta\theta^2\rangle\right)\frac{\mathbf{p}}{p},$$

$$\langle\Delta\mathbf{p}\Delta\mathbf{p}\rangle=p^2\langle\Delta\theta^2\rangle\left(\mathcal{I}-\frac{\mathbf{pp}}{p^2}\right),$$

for the fast electron probability density $f(\mathbf{r},\mathbf{p},t)$ [25], where $\langle\ \rangle$ signifies the mean change per second, $\mathcal{I}$ is the identity tensor, $\langle\Delta p\rangle$ is the drag term, $\langle\Delta\theta^2\rangle$ is the angular scattering term, and the other symbols have their usual meanings. There is no diffusion in the fast electron energy due to neglect of the motion of the background particles. Equation (1) is valid for fast electron speeds much greater than the mean speed of the background particles.

We require expressions for the drag and angular scattering terms for transport through solid density matter, at temperatures relatively low by plasma standards. So we will consider the terms for transport through solids. For electrons with energies from 10 keV to a few MeV the standard result for the drag term [26] is

$$\langle\Delta p\rangle\approx-\frac{Zne^4}{4\pi\varepsilon_0^2 mv^2}\ln\frac{K}{I_{\rm ex}}=-\frac{Zne^4}{4\pi\varepsilon_0^2 mv^2}\ln\Lambda_l, \tag{2}$$

where Z is the atomic number, n is the background atom number density, m is the electron mass, K is the fast electron kinetic energy, and $I_{\rm ex}$ is the mean excitation energy, which is determined by the binding of the atomic electrons. We use the values for $I_{\rm ex}$ given in [26]. At energies greater than a few MeV additional effects, such as radiation and the density effect correction, become important [26]. The only difference between Eq. (2) and the expression for a plasma is the appearance of $I_{\rm ex}$ in the logarithmic term.

Angular scattering will be caused by collisions with the atoms. An approximate model for the field of an atom is an exponentially screened potential, with a screening distance (a) given by $a\approx 4\pi\varepsilon_0\hbar^2/Z^{1/3}me^2$ [27]. The de Broglie wavelength ($\lambda_{\rm dB}$) of the fast electrons is much less than typical interatomic spacings, so the atoms may be considered as independent scattering centers. Using the first Born approximation for the scattering formula,

$$\langle\Delta\theta^2\rangle\approx\frac{Z^2ne^4}{2\pi\varepsilon_0^2}\frac{\gamma m}{p^3}\ln\frac{4\pi a}{\lambda_{\rm dB}}=\frac{Z^2ne^4}{2\pi\varepsilon_0^2}\frac{\gamma m}{p^3}\ln\Lambda_s, \tag{3}$$

where γ is the Lorentz factor. The Born approximation requires [27]

$$\frac{Z\alpha}{v/c}\ln\frac{\Lambda_s}{2}<1,$$

where α ($\approx 1/137$) is the fine structure constant, so this is not valid at high Z (typically >30). Angular scattering by electrons is neglected. The only difference between this and the treatment for a plasma is the appearance of a in place of the Debye length, which only appears in the logarithmic term and therefore makes only a small difference.

Changes in the density of the background electrons due to the presence of the fast electrons have been neglected, thus we require the fast electron number density to be much lower than that of the background.

To calculate the fields we need a model for the response of the background. As the background electrons are highly collisional compared to the fast electrons and have a temperature much lower than the fast electron energies, we use $\mathbf{E}=\eta\,\mathbf{j}_b$. Glinsky [21] discusses this approximation in more detail. Further, assuming that the background current balances the fast electron current ($\mathbf{j}_f$) gives

$$\mathbf{E}=-\eta\,\mathbf{j}_f. \tag{4}$$

This is used by Glinsky [21] and Bell *et al.* [23]. The currents will remain approximately in balance for a magnetic diffusion time [24]

$$t_B=\frac{\mu_0}{\eta}L^2, \tag{5}$$

where L is the radial scale length of variations in $\mathbf{j}_f$. Bell *et al.* justify this approach by estimating the energy in the magnetic field generated if the initial fast electron current is not canceled, finding it to be vastly greater than the energy of the fast electrons. We calculate the magnetic field from

$$\frac{\partial\mathbf{B}}{\partial t}=-\nabla\times\mathbf{E}=\nabla\times\eta\mathbf{j}_f. \tag{6}$$

This can be expressed as two separate terms, $\eta\nabla\times\mathbf{j}_f$ and $\nabla\,\eta\times\mathbf{j}_f$. The latter term is only present when there are variations in resistivity, which occur when the heating of the background is taken into account. In solving the field equations (4) and (6) we assume rotational symmetry.

The displacement current has been neglected, which is only important for short time scales of order $\varepsilon_0\eta$, while the return current establishes itself. The resistivity is assumed to be isotropic and linear. The main effect which could lead to anisotropy is the magnetic field. We only consider $\mathbf{j}_f$ perpendicular to $\mathbf{B}$ so this is not a problem, although the magnetic field could change the value of the resistivity. The resistivity will be linear (i.e., independent of the electric field) if the drift velocity of the electrons carrying the background return current is much less than their mean speed. This requires either the net drift velocity of the fast electrons to be small, which will be the case with strong angular scattering, or the fast electron number density to be much less than that of the electrons carrying the return current.

There is a further restriction on the maximum fast electron current for which the model is valid as a high current leads to rapid heating of the background (from ηj_f^2), violating the assumption that the fast electron speed is much greater than the mean speed of the background electrons. In this case the distinction between fast and background electrons rapidly vanishes and it would be better modeled by a PIC code. In such a case the electrons which then escape the heated region and enter the target could be modeled using the approach given here.

The geometry used does not allow for kink instabilities. Microinstabilities, such as two stream instabilities, are not modeled in this approach. The effect of microinstabilities could be approximately accounted for by a suitable choice of the resistivity.

We now consider aluminum targets ($Z=13$, $n=6\times10^{28}$ m^{-3}, $I_{\mathrm{ex}}=166$ eV) and spot diameters of 20 μm. We choose aluminum because its resistivity has been measured over a wide range of temperatures [28] and it is frequently used in experiments. Milchberg *et al.* [28] found the maximum resistivity of solid density aluminum to be approximately 2×10^{-6} Ω m. This and $L=10$ μm give $t_B=63$ ps [Eq. (5)] and $\varepsilon_0\eta=0.02$ fs. So for picosecond pulses, magnetic diffusion and the displacement current may be neglected.

The energy lost by the fast electrons goes into the magnetic field and heating of the background, which will change the resistivity. To calculate the resistivity we use a fit to the results of Milchberg *et al.* [28], given by

$$\eta=\frac{1}{5\times10^6(kT_b)^{-1}+170(kT_b)^{3/2}+3\times10^5}\ \Omega\ \mathrm{m}, \tag{7}$$

where kT_b is the background temperature in eV. Their measurements extend to temperatures just over 100 eV. Equation (7) reproduces the classical results of linear growth at low T_b and the $T_b^{3/2}$ dependence at high T_b. The fit is not good at temperatures less than 1 eV. It gives a maximum resistivity of $\approx2.2\times10^{-6}$ Ω m at $kT_b\approx53$ eV. To calculate the temperature from the energy loss we require the specific heat capacity. This is not well known for the conditions of interest and, in general, is a function of temperature. We use a fixed specific heat capacity, using the value for aluminum at room temperature. The mean number of free electrons per atom in aluminum remains close to three at temperatures up to 50 eV [28]. The ionization energy required to produce Al^{4+} is approximately 120 eV. Thus our model of the background will be sufficiently accurate for our purpose of evaluating the importance of a finite, variable resisitivity for background temperatures up to $kT_b\sim10^2$ eV. In calculating the background temperature, thermal conduction is neglected.

The target is assumed to be semi-infinite, with uniform density and, initially, uniform temperature, although these assumptions may easily be removed. A specified distribution of fast electrons is assumed to enter from the target surface, placed at $z=0$. Electrons are specularly reflected from this boundary, as in the model of Luther-Davies *et al.* [5]. This will be acceptable as long as the scale length of any plasma on the surface remains much less than the distances that the fast electrons travel. It is possible that a small number of high energy electrons could escape the target, particularly when high energy ion emission [1] starts to occur.

III. COMPUTATIONAL MODEL

We use the equivalence of Fokker-Planck equations to SDEs to solve Eq. (1) with a Monte Carlo–type method. This method is well established and there are many texts on the subject, e.g., [29]. It gives a particle approach to solving the Fokker-Planck equation. This type of approach is ideal for highly localized and anisotropic distributions, which are expected in laser plasma interactions. Finite element and finite difference approaches have difficulty with such distributions.

We use the Ito SDEs [29] formulated in terms of a particle's position ($\mathbf{r}$), magnitude of momentum (p), and scattering angle (θ). Neglecting the force from the fields for the present, this gives

$$d\mathbf{r}=\mathbf{v}dt, \tag{8}$$

$$dp=\langle\Delta p\rangle dt=-\frac{Zne^4}{4\pi\varepsilon_0^2 mv^2}\ln\Lambda_l dt, \tag{9}$$

$$d\theta=\langle\Delta\theta^2\rangle^{1/2}dW=\left(\frac{Z^2ne^4}{2\pi\varepsilon_0^2}\frac{\gamma m}{p^3}\ln\Lambda_s dt\right)^{1/2}\Gamma(t), \tag{10}$$

where dW is the increment of a Wiener (diffusion) process and $\Gamma(t)$ is a time varying random number with a Gaussian distribution, mean zero, and variance 1. Gaussian random numbers are generated using a Box-Muller transformation method [30]. Equation (8) is the standard equation of motion. Equation (9) represents a deterministic loss in the magnitude of an electron's momentum. These equations are solved numerically using a first order difference scheme. Equation (10) represents a random rotation in an electron's direction of motion, which is applied about an axis at a random angle perpendicular to the direction of motion. The rotation is evaluated exactly, using the previous momentum to calculate $d\theta$. The logarithmic terms are not assumed to be constant. The collisional part of the code is executed in three-dimensional Cartesian geometry.

The assumption of rotational symmetry allows nonzero $E_r(r,z)$, $E_z(r,z)$, and $B_\theta(r,z)$. The acceleration by the electric field is evaluated numerically using the same scheme used for Eqs. (8) and (9). The rotation about the magnetic field is calculated in a manner similar to the angular scattering [Eq. (10)]. The field equations (4) and (6) are solved on a uniform r-z grid, using centered spatial differencing and first order time differencing. The $r=0$ and $z=0$ boundaries are reflective and the fields are assumed to be zero at the far boundaries. The currents on the grid and the fields on the particles are found by using a linear weighting system between the four grid points nearest to a particle, as in standard PIC codes [31]. The magnetic field at the first two radial grid points is found by a linear fit from zero at $r=0$ to the value obtained at the third radial grid point. The electric field is smoothed over the first two radial grid points. This minimizes errors for particles near $r=0$.

The computational particles each represent a specified number of electrons. The particles are set up with a uniform distribution over the desired region of phase space (r,z,p_r,p_z) using the Sobel sequence number generator [30]. The particles are then assigned a number of electrons to give the desired electron number density. This assures good statistics over the whole phase space. Once an electron's energy falls below a certain level it will rapidly thermalize with the background, so particles with energy below a specified value are stopped.

The energy loss on the grid, required for the temperature calculation (Sec. II), is calculated by accumulating the energy lost by the particles in each time step in the grid cells they are in at that time step.

The various features of the code (collisions, electric field, magnetic field, variation of resistivity, and relativity) may be switched on and off and have all been tested independently. The collisional part has been tested against known solutions of the fast electron Fokker-Planck equation [32]. The purely collisional case has been extensively studied using this code [33]. Pinching and filamentary instabilities, described by Miller [24], have been reproduced in runs including only the fields and fixed resistivity.

IV. RESULTS

We consider a nominal laser intensity given by

$$I=I_p e^{-r^2/R^2}e^{-(t-t_p)^2/\tau^2} \tag{11}$$

with a spot diameter $2R=20$ μm, pulse length $2\tau=1$ ps, pulse peak at $t_p=1$ ps, and various values of I_p. For the fast electron temperature (kT_f) we use the result given by Beg *et al.* [34] and Lee [3], obtained from $K\alpha$ and bremsstrahlung emission measurements from picosecond, one micrometer wavelength laser solid experiments

$$kT_f=100\left(\frac{I\lambda^2}{10^{17}\ \mathrm{W\,cm^{-2}}}\right)^{1/3}\ \mathrm{keV}, \tag{12}$$

where we have included the usual wavelength scaling. They assumed a fast electron energy distribution e^{-K/kT_f}. Various calculations of the absorbed fraction gave values in the range 20–80 % [3]. Their results are space and time averaged and apply to the averaged intensity. Nevertheless we use Eq. (12) to obtain a space and time dependent $kT_f(r,t)$ from the intensity given by Eq. (11), which we then use to give the fast electron energy distribution $e^{-K/kT_f(r,t)}$. The energy flux of fast electrons ($n_f v kT_f$) is assumed to be 30% (f_{abs}) of the local, time dependent intensity.

The electrons are generated moving into the target at a random angle which is uniformly distributed in a cone of half angle 20° about the normal. That the electrons travel more or less straight into the target is in line with the results of Rousse *et al.* [7], Luther-Davies *et al.* [5], and Kieffer *et al.* [35].

From these parameters we can make estimates for the relative magnitudes of the various terms which affect the fast electron transport. Assuming that the resistivity is constant and the fast electrons enter parallel to the axis we have $E_z(r,t)=\eta e f_{\mathrm{abs}} I(r,t)/kT_f(r,t)$ at the target surface, if there is no return current of reflected fast electrons there. The maximum value of this electric field ($E_z(0,t_p)$) is

$$E_{\max}\approx 6\times 10^9\left(\frac{\eta}{2\times 10^{-6}\ \Omega\ \mathrm{m}}\right)\left(\frac{f_{\mathrm{abs}}}{0.3}\right)\times\left(\frac{I}{10^{17}\ \mathrm{W\,cm^{-2}}}\right)^{2/3}\left(\frac{1\ \mu\mathrm{m}}{\lambda}\right)^{2/3}\mathrm{V\,m^{-1}}. \tag{13}$$

Integrating $\partial E_z/\partial r$ from $t=0$ to ∞ gives the maximum magnetic field [Eq. (6)]

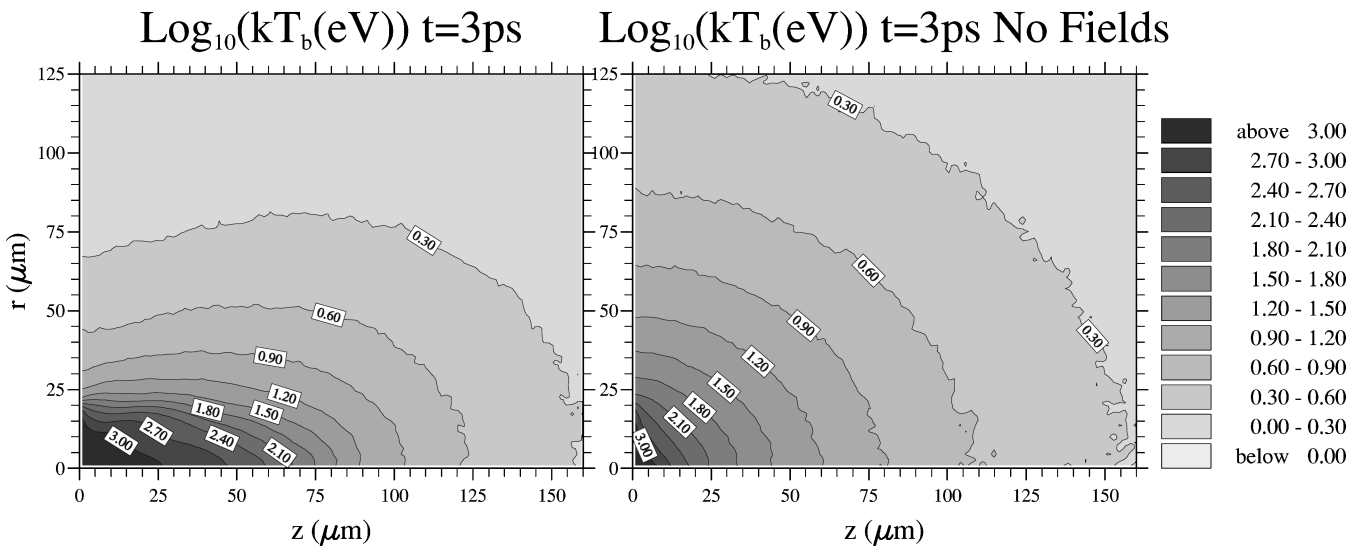

FIG. 1. Log_{10} of the temperature in eV after 3 ps. The maximum temperatures are 9.6 keV and 4.2 keV with only collisions.

$$B_{\max}\approx 230\left(\frac{\eta}{2\times 10^{-6}\ \ \Omega\,\mathrm{m}}\right)\left(\frac{2\tau}{1\ \ \mathrm{ps}}\right)\left(\frac{10\ \ \mu\mathrm{m}}{R}\right)\left(\frac{f_{\mathrm{abs}}}{0.3}\right)\times\left(\frac{\mathrm{I}}{10^{17}\ \ \mathrm{W\,cm^{-2}}}\right)^{2/3}\left(\frac{1\ \ \mu\mathrm{m}}{\lambda}\right)^{2/3}\mathrm{T} \tag{14}$$

at $r=\sqrt{3}R/2$. These upper limits on the fields could be raised by the pinching of the electron flow by the magnetic field. The magnetic field can also be increased by the $\nabla\eta\times\mathbf{j}_f$ term [Eq. (6)], if the resistivity increases with temperature. With the variation in resistivity switched off the code agrees well with these estimates, as long as the magnetic field does not get high enough for pinching and filamentation to be important.

The ratio of the force on the fast electrons from the magnetic field to that from the electric field is

$$\frac{vB_{\max}}{E_{\max}}=12\left(\frac{2\tau}{1\ \ \mathrm{ps}}\right)\left(\frac{10\ \ \mu\mathrm{m}}{\mathrm{R}}\right)\left(\frac{v}{c}\right), \tag{15}$$

where v is the fast electron speed. Hence the magnetic field is important and can be significant when the electric field is not.

To estimate the upper intensity at which the electric field may be neglected compared to the collisions, we compare the force from the maximum electric field [Eq. (13)] to the $\langle\Delta\mathbf{p}\rangle$ term [Eq. (1)]. They are equal when

$$I_p\approx 1.3\times 10^{17}\left(\frac{2\times 10^{-6}\ \ \Omega\,\mathrm{m}}{\eta}\right)\left(\frac{0.3}{f_{\mathrm{abs}}}\right)\left(\frac{n}{6\times 10^{28}\ \ \mathrm{m^{-3}}}\right)\times\left(\frac{1.5\gamma^2}{\gamma+1}\right)\left(\frac{Z}{13}\right)\left(\frac{\ln\Lambda_l}{6}\right)\left(\frac{1+Z\ln\Lambda_s/\gamma\ln\Lambda_l}{10}\right)\mathrm{W\,cm^{-2}}, \tag{16}$$

where we have substituted numbers suitable for aluminum and a fast electron kinetic energy of 100 keV. Both γ and the logarithmic terms depend on $I_p\lambda^2$, but only weakly. $\langle\Delta\mathbf{p}\rangle$ increases as the electrons slow down while E decreases, so for intensities less than this the electric field could be neglected. However, pinching of the electron flow by the magnetic field could increase the maximum electric field thus decreasing this intensity. This threshold intensity agrees well with that given by Bell *et al.* [23], although the derivation differs.

To estimate the upper intensity at which the magnetic field may be neglected compared to the collisions, we compare the force from the maximum magnetic field [Eq. (14)] with the angular scattering contribution in the $\langle\Delta\mathbf{p}\rangle$ term [$p\langle\Delta\theta^2\rangle/2$, Eq. (1)] giving

$$I_p\approx 2.0\times 10^{16}\left[\left(\frac{2\times 10^{-6}\ \ \Omega\,\mathrm{m}}{\eta}\right)\left(\frac{1\ \ \mathrm{ps}}{2\tau}\right)\left(\frac{R}{10\ \ \mu\mathrm{m}}\right)\left(\frac{0.3}{f_{\mathrm{abs}}}\right)\times\left(\frac{n}{6\times 10^{28}\ \ \mathrm{m^{-3}}}\right)\left(\frac{1\ \ \mu\mathrm{m}}{\lambda}\right)^{1/3}\left(\frac{2.8\gamma^2}{(1+\gamma)^{3/2}}\right)\times\left(\frac{Z}{13}\right)^2\left(\frac{\ln\Lambda_s}{5}\right)\right]^{6/7}\mathrm{W\,cm^{-2}}. \tag{17}$$

Using the maximum value of the resistivity this gives the intensity below which a purely collisional model should be accurate.

To check if this rough evaluation of when the fields can be neglected is accurate, we performed a run with $I_p=10^{17}$ $\mathrm{W\,cm^{-2}}$, $\lambda=1\ \ \mu$m, and an initial temperature of 53 eV, at which $\eta=2.2\times 10^{-6}\ \ \Omega$ m and decreases with temperature. The fast electrons lost 99.6% of their total energy over 3 ps, 8.7% of this loss was due to the electric field. The magnetic field reduced the mean radial spread of the fast electrons after 3 ps by 32% from the purely collisional result. The electric field reduced the mean penetration depth by 10%. The penetration depth of intermediate energy electrons was increased slightly by the magnetic field. The maximum magnetic and electric fields were 240 T and 3.6×10^9 $\mathrm{V\,m^{-1}}$, respectively. This is lower than the values from Eqs. (13) and (14) (253 T and 6.6×10^9 $\mathrm{V\,m^{-1}}$) because the resistivity drops. With the variation in resistivity switched off the pinching of the electron flow significantly increased the

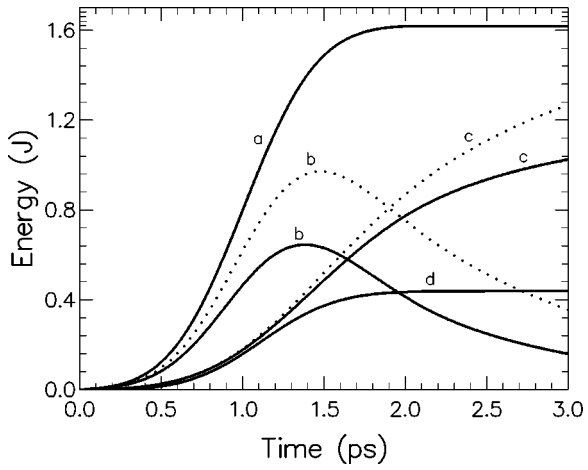

FIG. 2. (a) Energy absorbed, (b) kinetic energy, (c) energy loss due to collisions, (d) energy loss due to the electric field. Dotted lines are for the run including only collisions.

fields, giving maximum fields of $1.2kT$ and 1.1×10^{10} V m^{-1}. In contrast with $I_p=10^{16}$ W cm^{-2}, the energy loss due to the electric field was only 0.2% of the total energy and the magnetic field both decreased the mean radial spread and increased the mean penetration depth by around 10%. As predicted by the estimates above, the electric field is not a major effect at intensities of 10^{16} and 10^{17} W cm^{-2} and the magnetic field is only significant at the higher intensity.

We will now consider, in some detail, a run with $I_p=2\times10^{18}$ W cm^{-2}, $\lambda=1$ μm, and an initial temperature of 1 eV, giving $\eta=1.9\times10^{-7}$ Ω m. This corresponds to experiments at quoted intensities of $\approx 10^{18}$ W cm^{-2} (due to averaging) and with a prepulse sufficient to preheat the target but not to cause large scale hydrodynamic motion. For comparison, some results from a run including only the collisions are given. At this intensity all the effects are expected to be important.

The grid was 270 μm in radius and 400 μm thick, the grid spacings were 1.8 μm in r and z, the time step was 0.006 ps, and the code was run for 3 ps. 2800 computational particles (each representing a different number of electrons, see Sec. III) were generated per time step for the first 2 ps. The maximum number of computational particles on the grid was just over 5×10^5. Electrons were stopped when their energy fell below 10 keV, when their collisional stopping distance is 1.3 μm [26].

First we consider whether the results are consistent with the approximations used. The neglect of the displacement current means that the energy in the electric field ($\varepsilon_0E^2/2$) is assumed to be zero, in the code its maximum value is 1.6×10^{-4}% of the total energy, so the neglect is consistent. To check the assumption of current balance we compare the magnetic field in the code to that given by $\nabla\times\mathbf{B}=\mu_0\mathbf{j}_f$, the code value is at maximum 1% of this value indicating that current balance is maintained to within 1%. To evaluate the neglect of magnetic diffusion we estimate the magnetic diffusion time [Eq. (5)] from plots of the resistivity and magnetic field, its minimum value is $\approx$5.7 ps justifying the neglect for 3 ps. The fast electron number density is assumed to be much less than that of the background, the maximum fast electron number density in the code is just under half that of aluminum's atom number density, thus the assumption is justified. If the peak intensity were increased to 10^{19} W cm^{-2} this would be violated. To check the assumption of linear resistivity we calculate the background electron drift speed assuming three conduction electrons per atom, at maximum this is 7.2×10^5 ms^{-1} (kinetic energy 1.5 eV) at a point

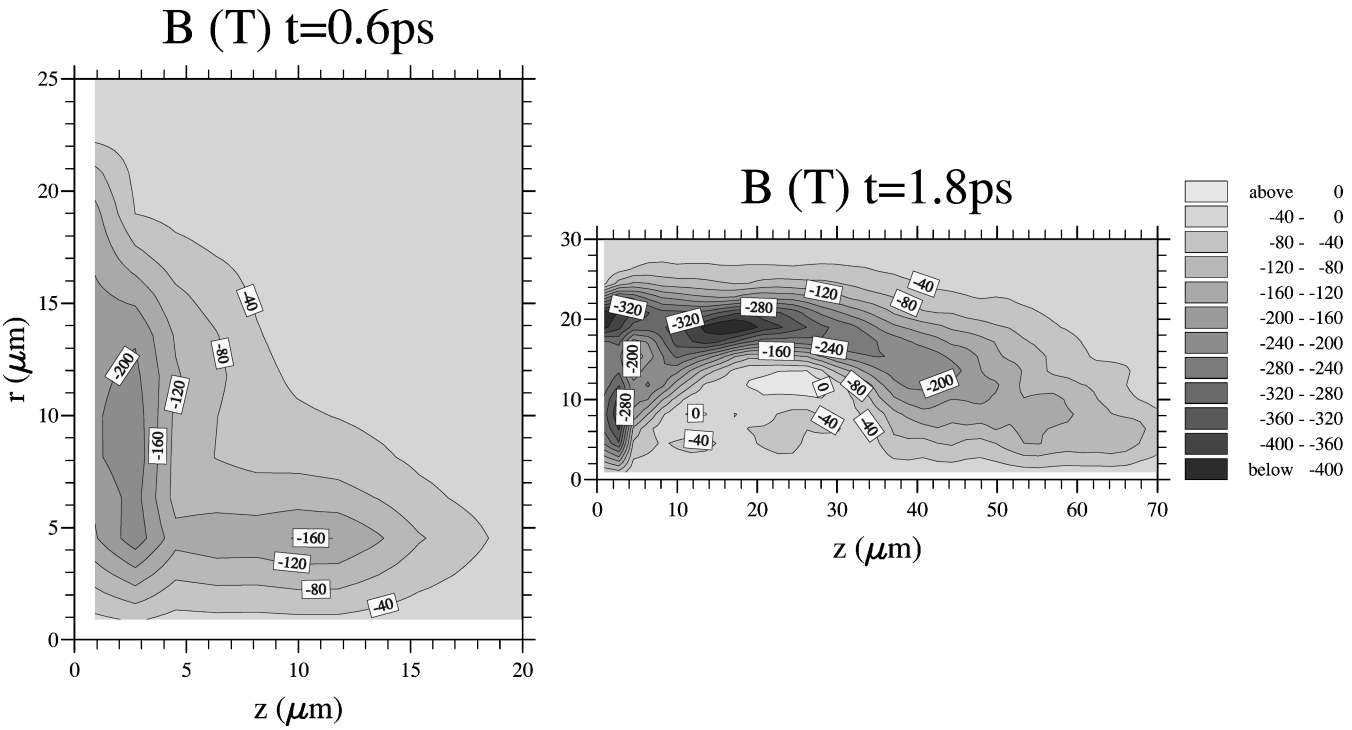

FIG. 3. Magnetic field in teslas. The maximum magnetic field reached is 454 T (4.54 MG) at 1.8 ps. The maximum field is $\approx$6% lower by 3 ps.

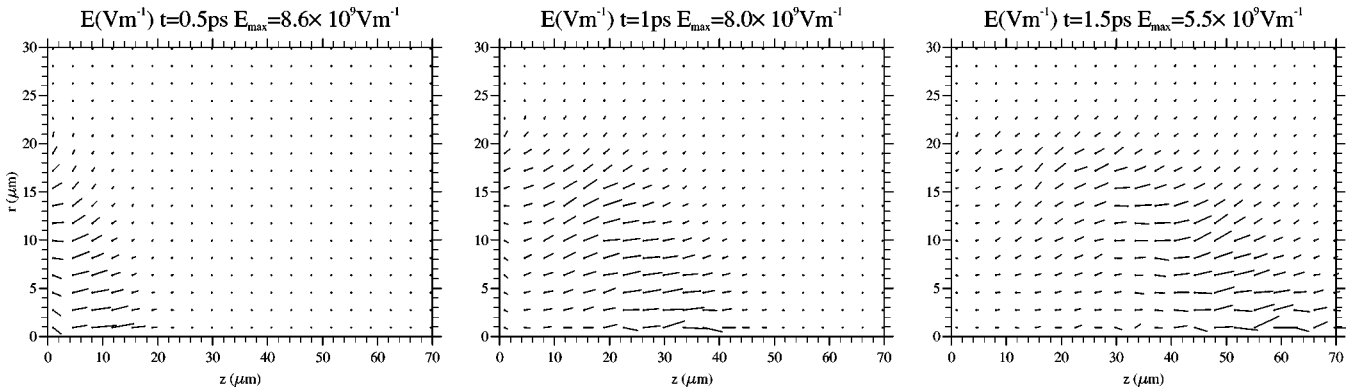

FIG. 4. Vector plots of electric field. Dots indicate origins of vectors, the lines extend in the direction of the field, their length being proportional to the magnitude. The magnitude of the largest vector shown is given. Every vector in r and every second one in z are plotted. The maximum electric field generated is 1.1×10^{10} V m^{-1} at 0.8 ps.

where the background temperature is 6 keV and the electric field is negligible. In regions where the electric field is significant the background electron drift speeds are much less than 10^5 ms^{-1}, justifying the assumption of linear resistivity. The treatment of the background requires it to remain relatively cold, by 3 ps a small region behind the laser spot has reached temperatures >1 keV (Fig. 1), when the neglect of ionization and hydrodynamics is not justified, and a roughly conical region of maximum radius 20 μm and depth 60 μm has been heated to temperatures >200 eV at which point the background model starts to break down. Ablation, ionization, and heat transport would reduce these temperatures. The calculation of the fast electron transport at earlier times and greater distances in the target will not be significantly in error. The high degree of heating near the target surface is the main source of error in the model.

The energy gain in the code over the course of the run was 0.28%. Runs with a range of time steps showed that the energy error per time step scaled as dt^2, as would be expected. Decreasing the time step by a factor of 7 made no difference to the overall results.

The fast electron energy loss caused by the electric field is calculated in two ways: (i) from the change in energy of the particles given by the difference equations and (ii) from $\mathbf{j}_f\cdot\mathbf{E}$ on the grid. Method (ii) gives results which are at most 5.5% greater than method (i), indicating that the fields and currents are well resolved by the grid. Increasing the grid spacings to 2 μm made no difference in the overall results.

By the end of the run particles have reached 618 μm in r and 600 μm in z, which is outside the grid used for the field calculations. However, the fields are negligible well short of the boundaries so this does not cause any significant error. Moving the boundaries did not change the results. Particles leaving the grid are included in all other calculations.

We now consider the implications of the results. 90% of the absorbed energy has been lost by the end of the run (Fig. 2), compared to 78% with only collisions included. 70% of the energy loss is due to collisions (this includes the energy of electrons that are stopped) and 30% is due to the electric field. Thus the electric field is an important energy loss mechanism. The energy loss due to the electric field is most important at early times and almost zero at later times (>2 ps), as predicted by Glinsky [21]. Thus the electric field lowers the energy of the electrons before they spread through the target. The maximum energy in the magnetic field is 0.11% of the total energy, so the bulk of the energy lost by the fast electrons heats the background.

The fast electrons can roughly be divided into three cat-

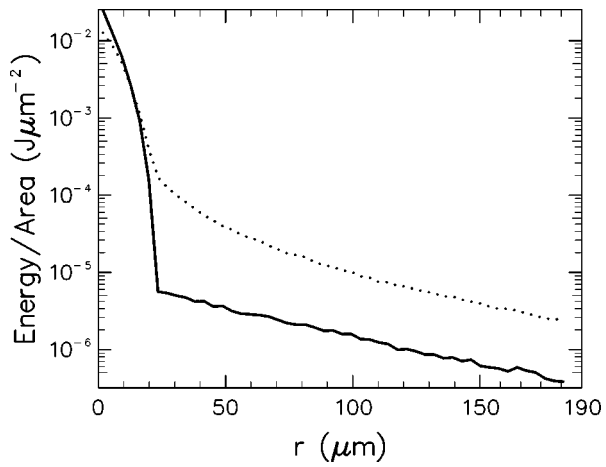

FIG. 5. Radial distribution of total energy reflected from the target surface over 3 ps. Dotted line is for the run with collisions only.

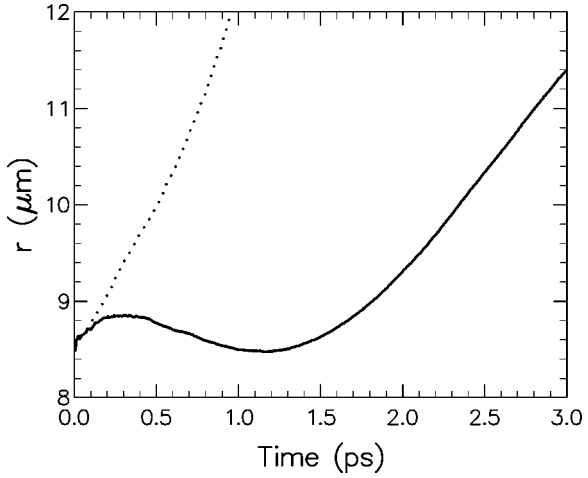

FIG. 6. Energy weighted mean radius of electrons reflected from the target surface by a given time. Dotted line is for the run with collisions only; it continues upwards to 36 μm.

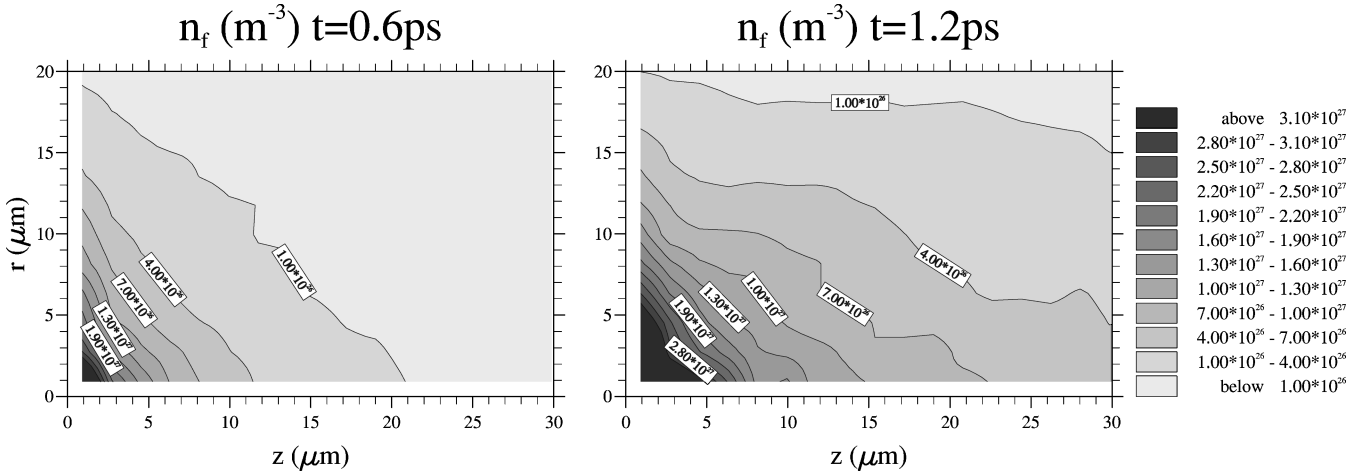

FIG. 7. Number density of fast electrons, excluding the stopped electrons, in the region behind the laser spot.

egories, determined by their energy.

(i) Low energy electrons (<40 keV). These rapidly lose their energy to the electric field and collisional drag, heating a thin layer behind the spot (Fig. 1). They account for the temperature in the grid cells directly behind the spot being much higher than elsewhere.

(ii) Intermediate energy electrons. Their transport is dominated by the fields that they generate. These dominate the heating and field generation for $r<20$ μm and $z<80$ μm (Figs. 1, 3, and 4).

(iii) High energy electrons, on the tail of the energy distribution. Their low number density means they do not contribute significantly to the field generation. They lose some of their energy to the electric field, typically around 40 keV, and are deflected radially inwards by the magnetic field near the spot (Fig. 3), then spread rapidly through the target. These account for the results further into the target having the same pattern as the collisional results, but characterized by a lower fast electron energy.

The division between these categories is not particularly distinct due to the radial and time variation in the fast electron temperature and density. It is further complicated by the magnetic field being a time integrated effect.

To determine the importance of the reflective boundary at the target surface, radial distributions of the energy, number, and angle of incidence of reflected electrons are calculated. The total number of electrons reflected over 3 ps is 32% of the total number, compared to 28% for the run including only collisions. This increase is due to the magnetic field. A few particles are reflected more than once. Hence the reflective boundary at the target surface has a significant effect. The distribution of the reflected energy (Fig. 5) is strongly peaked at $r<20$ μm due to lower energy electrons reflected by magnetic field and angular scattering. At larger r a small number of higher energy electrons are returned to the surface by angular scattering; the magnetic field is negligible at $r>30$ μm (Fig. 3). The radius at which the majority of high energy electrons are returned to the surface by angular scattering and the time before they return increase with the electron energy [33]. Thus the radius at which the bulk of the electrons is reflected increases late in time (Fig. 6). The energy weighted mean radius of reflection (Fig. 6) decreases at early times due to the electrons reflected by the magnetic field. The x-rays that these high energy electrons would generate as they are reflected could explain the x-ray emission around the laser spot detected from the front of solid targets in some experiments, e.g., [36–39]. The reason Bur-

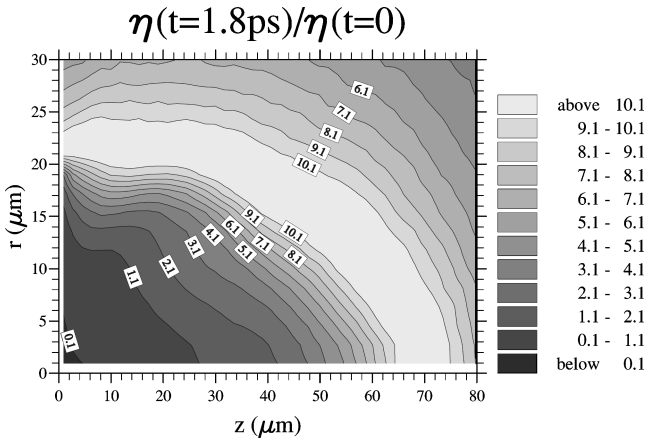

FIG. 8. Resistivity at $t=0$ is 1.9×10^{-7} Ω m. Maximum resistivity is 2.2×10^{-6} Ω m. Lowest resistivity is 4.0×10^{-9} Ω m.

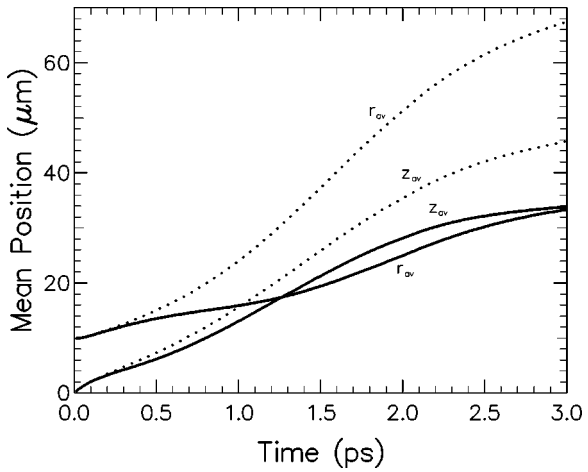

FIG. 9. Mean position of all the fast electrons, including stopped electrons. The initial value of r_{av} is set by the assumed spot radius [R in Eq. (11)]. Dotted lines are for the run including only collisions.

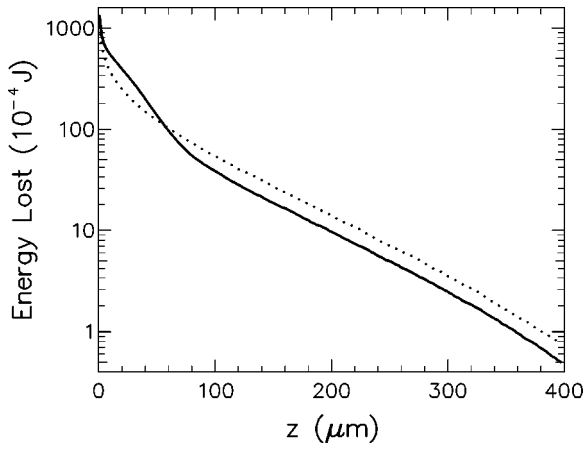

FIG. 10. r integrated distribution of energy loss on the grid after 3 ps. Dotted line is for the run including only collisions.

gess *et al.* [37] detected a clear ring in their time integrated measurements, where others just find an increase in the x-ray emission region over the spot size, may be due to the very small spot size (~ 1 μm) resulting in a clear separation between the generation region and the radius at which the fast electrons return to the surface. This provides an additional mechanism for the lateral transport of fast electrons to the coronal transport mechanisms previously considered, e.g., [18].

We will now concentrate on the intermediate energy electrons. At early times the fields are not significant and the fast electrons move inwards at a speed which is greater near the axis, as the intensity is higher there, thus the electrons penetrate further nearer the axis, as can be seen in Fig. 7. The effect of this early time variation in penetration can be seen in the position of the leading edge of the magnetic (Fig. 3) and electric (Fig. 4) fields. As the intensity and, initially, the resistivity increase, the electric field becomes significant and the higher intensity near the axis now leads to greater inhibition of the electron flow there, reducing the electron penetration near the axis, as can be seen in the plot of the electron number density at 1.2 ps (Fig. 7). This is why the temperature (Fig. 1), fields (Figs. 3 and 4), and resistivity (Fig. 8) behind the laser spot do not vary so strongly with radius closer to the target surface. In a run including only the electric field (fixed resistivity, no magnetic field or collisions) the electrons penetrated significantly further at larger r. This does not occur here as the greater heating near the axis eventually lowers the resistivity there and hence the electric and magnetic fields (Figs. 3, 4, and 8). The eventual lowering of the resistivity allows the intermediate energy electrons to penetrate further than if the resistivity were fixed. As can be seen from Fig. 4, the region of maximum electric field moves inwards in time, this maximum corresponding to the peak in the resistivity. As the magnetic field builds up it pinches the electron flow reducing the radial spread (Fig. 9) and increasing the penetration depth of intermediate energy electrons from the purely collisional case. The effect of this pinching can be seen in the temperature plots (Fig. 1). The mean radial spread of the fast electrons over 3 ps is 59% lower than for the purely collisional case (Fig. 9). The mean penetration depth (Fig. 9) after 3 ps is 26% lower than the purely collisional case due to the electric field slowing the electrons. Runs excluding the electric field showed an increased mean penetration depth over the collisional result. As mentioned in Secs. II and III the magnetic field can cause filamentation. However, a number of effects act to prevent this here: (i) the increased current density in a filament leads to an increased electric field which acts to stop the fast electron flow in the filament, (ii) the angular scattering acts to spread out the fast electrons, and (iii) the spread in the generated fast electron distribution opposes filamentation. The action of each of these effects in reducing filamentation has been observed in test runs with the other effects turned off.

The higher electric field on axis could, at least partly, explain the lower x-ray emission at small r from the back of the layered targets found by Luther-Davies *et al.* [5], as mentioned by Bell *et al.* [23]. The lack of low energy electrons in the fast electron distribution obtained by Luther-Davies *et al.* [5] can be explained by the electric and magnetic fields preventing low energy electrons penetrating and the enhancing of the penetration of intermediate energy electrons by the magnetic field, as they mention.

The patterns of the fields at times >1 ps are dominated by the changes in resistivity, as can be seen by comparing the plot of resistivity (Fig. 8) with the field plots (Figs. 3 and 4). The resistivity just behind the spot becomes so low that the electric field becomes negligible and the magnetic field there ceases to change. The $\nabla\eta\times\mathbf{j}_f$ term [from Eq. (6)] causes the magnetic field inside the region of peak resistivity (Fig. 8) to fall and eventually to change sign (Fig. 5). Hence the inclusion of self-consistent resistivity significantly changes the results. This limits the applicability of the model of Bell *et al.* [23] where the resistivity was fixed.

For the determination of fast electron temperatures from $K\alpha$ emission measurements from layered targets an important parameter is the energy lost at a given depth. Figure 10 gives the z distribution of the fast electron energy loss after 3 ps. The energy loss in the purely collisional case is lower for $z<55$ μm and on average 42% higher for $z>80$ μm. The curves are roughly the same shape at $z>80$ μm as the transport of the high energy electrons is collision dominated, the lower value is from the energy loss of the fast electrons as they pass the electric field at low z. Thus purely collisional models will underestimate the energy and number of fast electrons generated.

The calculation with $I_p=2\times10^{18}$ W cm^{-2} has been repeated with an initial temperature of 10 eV, giving $\eta=1.2\times10^{-6}$ Ω m. As the temperature (Fig. 1) in the region where the fields are important is dominated by the fast electron heating, the change in initial temperature does not have a large overall effect. The energy loss due to the electric field was increased by 4.8%, resulting in the fast electrons losing 91% of their total energy in 3 ps. The mean radius of the fast electrons after 3 ps was reduced by 4.8% and the mean penetration depth by 0.4%. Thus the results in this case are not strongly dependent on the initial temperature.

V. CONCLUSIONS

We have shown that electric and magnetic fields and variable resistivity, as well as collisions, can all play an important role in fast electron transport through solid targets. The

noncollisional effects are most important at high intensities and resistivities. The magnetic field is higher in calculations with tighter focal spots and longer pulses.

The electric field lowers the energy of the electrons as they enter the target. The subsequent transport of the electrons which are not stopped is determined by the collisions and the magnetic field. The magnetic field reflects lower energy electrons and acts to funnel in the intermediate energy electrons. The highest energy electrons on the tail of the energy distribution lose some of their energy due to the electric field and are deflected radially inwards by the magnetic field near the target surface. Then they move rapidly through the target, unaffected by the fields, spreading out due to angular scattering. The eventual decrease in resistivity as the target is heated increases the penetration of intermediate energy electrons. The variations in resistivity significantly affect the magnetic field generation through the $\nabla\eta\times\mathbf{j}_f$ term [Eq. (6)]. This dependence on resistivity introduces a strong material dependence to the fast electron transport, as the magnitude and temperature dependence of resistivity vary significantly for different materials, e.g., the range of resistivities at room temperature covers around 20 orders of magnitude.

The results obtained here indicate that the fraction of absorbed energy carried large distances ahead of the ablation front by fast electrons will be lower at higher intensities and resistivities. Effectively the inclusion of finite resistivity puts a limit on the fast electron current which can penetrate the target.

The purely collisional interpretations of fast electron transport in $K\alpha$ emission experiments that have been used previously will underestimate the number and energy of fast electrons. This could explain some of the rather low results that have been obtained at high intensities [5,7,9,40], as discussed by Bell *et al.* [23].

The major drawback of the code described here as a predictive tool is the need to specify the fast electron distribution, the background resistivity, and specific heat capacity, which are not well known parameters in laser solid experiments. More work needs to be done to determine these.

The transport of fast electrons is of critical importance in the fast igniter concept [19]. There are two major problems in using the code described here to model the fast igniter: (i) the high intensities proposed for the ignition pulse are likely to generate a very high flux of fast electrons possibly violating the requirement that the fast electron number density be much less than that of the background, and (ii) the behavior of the background will be more complicated than the simple model used here. There are also problems in specifying the resistivity; microinstabilities are likely to play an important role [24]. The implications of electric field generation for the fast igniter have been discussed by Tabak *et al.* [19] and Bell *et al.* [23]. The collimation of the fast electron flow by the magnetic field would be beneficial to this scheme increasing the energy reaching the core, as mentioned by Tabak *et al.* [19].

More work needs to be done on the effects of field generation. To be more generally applicable the model presented here must be extended to include magnetic diffusion and a more realistic treatment of the background.

ACKNOWLEDGMENTS

This work was supported by U.K. EPSRC Grant No. GR/K19198 and SILASI European Network ERB 4061 PL 95-0765.

[1] S. J. Gitomer, R. D. Jones, F. Begay, A. W. Ehler, J. F. Kephart, and R. Kristal, Phys. Fluids **29**, 2679 (1986).
[2] P. Gibbon and E. Förster, Plasma Phys. Controlled Fusion **38**, 769 (1996).
[3] P. Lee C. K., Ph.D. thesis, University of London, 1996.
[4] J. D. Hares, J. Kilkenny, M. H. Key, and J. G. Lunney, Phys. Rev. Lett. **42**, 1216 (1979).
[5] B. Luther-Davies, A. Perry, and K. A. Nugent, Phys. Rev. A **35**, 4306 (1987).
[6] H. Chen, B. Soom, B. Yaakobi, S. Uchida, and D. D. Meyerhofer, Phys. Rev. Lett. **70**, 3431 (1993).
[7] A. Rousse, P. Audebert, J. P. Geindre, F. Fallies, J. C. Gauthier, A. Mysyrowicz, G. Grillon, and A. Antonetti, Phys. Rev. E **50**, 2200 (1994).
[8] D. D. Meyerhofer, H. Chen, J. A. Delettrez, B. Soom, S. Uchida, and B. Yaakobi, Phys. Fluids B **5**, 2584 (1993).
[9] Z. Jiang, J. C. Kieffer, J. P. Matte, M. Chaker, O. Peyrusse, D. Gilles, G. Kom, A. Maksimchuk, S. Coe, and G. Mourou, Phys. Plasmas **2**, 1702 (1995).
[10] P. Audebert, J. P. Geindre, J. C. Gauthier, A. Mysyrowicz, J. P. Chambaret, and A. Antonetti, Europhys. Lett. **19**, 189 (1992).
[11] O. L. Landen, E. M. Campbell, and M. D. Perry, Opt. Commun. **63**, 253 (1987); D. G. Stearns, O. L. Landen, E. M. Campbell, and J. H. Scofield, Phys. Rev. A **37**, 1684 (1988).
[12] M. Chaker, J. C. Kieffer, J. P. Matte, H. Pepin, P. Audebert, P. Maine, D. Strickland, P. Bado, and G. Mourou, Phys. Fluids B **3**, 167 (1991).
[13] M. Schnürer, M. P. Kalashnikov, P. V. Nickles, T. Schlegel, W. Sander, N. Demchenko, R. Nolte, and P. Ambrosi, Phys. Plasmas **2**, 3106 (1995).
[14] G. Guethlein, M. E. Foord, and D. Price, Phys. Rev. Lett. **77**, 1055 (1996).
[15] L. V. Spencer, Phys. Rev. **98**, 1597 (1955).
[16] J. M. Wallace, D. W. Forslund, J. M. Kindel, G. L. Olson, and J. C. Comly, Phys. Fluids B **3**, 2337 (1991).
[17] W. S. Lawson, P. W. Rambo, and D. J. Larson, Phys. Plasmas **4**, 788 (1997).
[18] J. M. Wallace, J. U. Brackbill, and D. W. Forslund, J. Comp. Phys. **63**, 434 (1986); D. W. Forslund and J. U. Brackbill, Phys. Rev. Lett. **48**, 1614 (1982).
[19] M. Tabak, J. M. Hammer, M. E. Glinsky, W. L. Kruer, S. C. Wilks, and J. Woodworth, Phys. Plasmas **1**, 1626 (1994).
[20] R. J. Mason and C. W. Cranfill, IEEE Trans. Plasma Sci. **14**, 45 (1986).
[21] M. E. Glinsky, Phys. Plasmas **2**, 2796 (1995).

[22] G. B. Zimmerman and W. L. Kruer, Comments Plasma Phys. Control. Fusion **2**, 51 (1975).
[23] A. R. Bell, J. R. Davies, S. Guerin, and H. Ruhl, Plasma Phys. Control. Fusion **39**, 653 (1997).
[24] R. B. Miller, *An Introduction to the Physical Intense Charged Particle Beams* (Plenum Press, New York, 1982), Chap. 4.
[25] See, for example, T. J. M. Boyd and J. J. Sanderson, *Plasma Dynamics* (Nelson, London, 1969), Chap. 10, the relativistic generalization is straightforward by expressing the equation in terms of momentum instead of velocity.
[26] International Committee on Radiation Units Report No. 37 (I.C.R.U., 1984).
[27] C. J. Joachain, *Quantum Collision Theory*, 3rd ed. (North-Holland, Amsterdam, 1987).
[28] H. M. Milchberg, R. R. Freeman, S. C. Davey, and R. M. More, Phys. Rev. Lett. **61**, 2364 (1988).
[29] See, for example, C. W. Gardiner, *Handbook of Stochastic Methods*, 2nd ed. (Springer-Verlag, Berlin, 1985); H. Risken, *The Fokker-Planck Equation*, 2nd ed. (Springer-Verlag, Berlin, 1984).
[30] W. H. Press, S. A. Teukolsky, W. T. Vettering, and B. P. Flannery, *Numerical Recipes*, 2nd ed. (Cambridge University Press, Cambridge, 1992).
[31] R. W. Hockney and J. W. Eastwood, *Computer Simulation Using Particles* (McGraw-Hill, New York, 1981).
[32] A. L. MacKinnon and I. J. D. Craig, Astron. Astrophys. **251**, 693 (1991).
[33] J. R. Davies, Ph.D. thesis, University of London, 1997.
[34] F. N. Beg, A. R. Bell, A. E. Dangor, C. N. Danson, A. P. Fews, M. E. Glinsky, B. A. Hammel, P. Lee, P. A. Norreys, and M. Tatarakis, Phys. Plasmas **4**, 447 (1996).
[35] J. C. Kieffer, H. Pépin, M. Piché, J. P. Matte, T. W. Johnston, P. Lavigne, F. Martin, and R. Decoste, Phys. Rev. Lett. **50**, 1054 (1983).
[36] J. A. Cobble, G. A. Kyrala, A. A. Hauer, A. J. Taylor, C. C. Gomez, N. D. Delamater, and G. T. Schappert, Phys. Rev. A **39**, 454 (1989).
[37] M. D. J. Burgess, B. Luther-Davies, and K. A. Nugent, Phys. Fluids **28**, 2286 (1985).
[38] F. Amiranoff, K. Eidmann, R. Sigel, R. Fedosejevs, A. Maaswinkel, Yung-lu Teng, J. D. Kilkenny, J. D. Hares, D. K. Bradley, B. J. MacGowan, and T. J. Goldsack, J. Phys. D **15**, 2463 (1982).
[39] P. A. Jaanimagi, N. A. Ebrahim, N. H. Burnett, and C. Joshi, Appl. Phys. Lett. **38**, 734 (1981).
[40] G. A. Kyrala, R. D. Fulton, E. K. Wahlin, L. A. Jones, G. T. Schappert, J. A. Cobble, and A. J. Taylor, Appl. Phys. Lett. **60**, 2195 (1992).